Value-Directed Human Behavior Analysis from Video Using Partially Observable Markov Decision Processes

Jesse Hoey and James J. Little, *Member*, *IEEE*

Abstract—This paper presents a method for learning decision theoretic models of human behaviors from video data. Our system learns relationships between the movements of a person, the context in which they are acting, and a utility function. This learning makes explicit that the meaning of a behavior to an observer is contained in its relationship to actions and outcomes. An agent wishing to capitalize on these relationships must learn to distinguish the behaviors according to how they help the agent to maximize utility. The model we use is a partially observable Markov decision process, or POMDP. The video observations are integrated into the POMDP using a dynamic Bayesian network that creates spatial and temporal abstractions amenable to decision making at the high level. The parameters of the model are learned from training data using an a posteriori constrained optimization technique based on the expectation-maximization algorithm. The system automatically discovers classes of behaviors and determines which are important for choosing actions that optimize over the utility of possible outcomes. This type of learning obviates the need for labeled data from expert knowledge about which behaviors are significant and removes bias about what behaviors may be useful to recognize in a particular situation. We show results in three interactions: a single player imitation game, a gestural robotic control problem, and a card game played by two people.

Index Terms—Face and gesture recognition, video analysis, motion, statistical models, clustering algorithms, machine learning, parameter learning, control theory, dynamic programming.

1 Introduction

This paper describes a model of human behaviors that unifies computer vision and decision theory through a framework of probabilistic modeling. The motivation is that computational agents will need capabilities for learning, recognizing, and using the extensive range of human nonverbal communication skills. The perceiver of a nonverbal signal must not only *recognize* the signal, but must *understand* what it is useful for. The signal's usefulness will be defined by its relationship to both signaler and receiver, their actions, their possible futures together, and the individual ways they assign value to these futures. This paper describes a method for the automatic learning and analysis of purposeful, context-dependent, human nonverbal behavior. No prior knowledge about the structure of behaviors or the number of behaviors is necessary. The method learns which behaviors (and how many) are conducive to achieving value in the context. An important aspect of our work is the explicit modeling of uncertainty in both the observations and in the temporal dynamics of the system. Taking this uncertainty into account allows the system to better optimize over possible outcomes based on noisy visual data. This paper will focus on human nonverbal communicative behaviors, including facial expressions and hand gestures. We will use the term *display* to refer to face or hand behaviors.

There has been a growing body of work in the past decade on the communicative function of the face [24], [46] and of the hands [38]. This psychological research has drawn three major conclusions. First, displays are often purposeful communicative signals [24]. Second, the purpose is not defined by the display alone, but also depends on the context in which the display was emitted [46]. Third, the signals are not universal, but vary between individuals in their physical appearance, their contextual relationships, and their purpose [46]. We believe that these three considerations should be used as critical constraints in the design of computational communicative agents able to learn, recognize, and use human behavior. First, context dependence implies that the agent must model the relationships between the displays and the context. Second, the agent must be able to compute the utility of taking actions in situations involving purposeful displays. Third, the agent needs to adapt to new partners and new situations.

These constraints can be integrated into a decision-theoretic, vision-based model of human nonverbal signals. The model can be used to predict human behavior or to choose actions that maximize expected utility. The basis for this model is a partially observable Markov decision process, or POMDP [1]. A POMDP describes the effects of an agent's actions upon its environment, the utility of states in the environment, and the relationship between the observations, the actions, and the states. A POMDP model allows an agent to predict the long term effects of its actions upon its environment and to choose valuable actions based on these predictions. The model can be acquired from data and can be used for decision making based, in part, on the nonverbal behavior of a human through observation.

- *J. Hoey is with the School of Computing, University of Dundee, Queen Mother Building, Dundee, Scotland, DD1 4HN. E-mail: jessehoey@computing.dundee.ac.uk.*
- *J.J. Little is with the Department of Computer Science, University of British Columbia, ICCS 117, 2366 Main Mall, Vancouver, B.C., Canada, V6T 1Z4. E-mail: little@cs.ubc.ca.*

Manuscript received 15 July 2004; revised 22 June 2005; accepted 29 Sept. 2006; published online 18 Jan. 2007.
Recommended for acceptance by I.A. Essa.
For information on obtaining reprints of this article, please send e-mail to: tpami@computer.org, and reference IEEECS Log Number TPAMI-0358-0704.
Digital Object Identifier no. 10.1109/TPAMI.2007.1145.

Our work is distinguished from other work on recognizing human nonverbal behavior primarily because it automatically learns what behaviors are distinguishable in the data and useful in the task. We do not train classifiers for predefined behaviors and then base decisions upon the classifier outputs. Instead, the training process *discovers* categories of behaviors in the data. This method is general in that it removes the need to reengineer a model for each task. This is especially important in the design of human-interactive systems since the human behaviors that will be observed are typically poorly known at the time of model specification. Instead, our method does not require expert knowledge about which displays are important nor extensive human labeling of data. Expert data labeling is not only time consuming, but also unnecessarily constrains the resulting models to the types of behaviors believed to be important by the experts.

In contrast, the Facial Action Coding System (FACS) has become the standard for psychological inquiries into facial expression. Computer vision researchers have made significant progress toward automatic FACS coding [2], [21], [55]. However, although the recognition of facial action units may give the ability to discriminate between very subtle differences in facial motion, or "microactions," it requires extensive training and domain specific knowledge [2]. Further, the importance of such a detailed level of representation is not clear for computer vision systems that intend to take actions based on observations of humans [42] and much simpler representations will be sufficient in many tasks. Our method takes a more task-oriented approach, automatically finding and modeling behaviors that are sufficient for performance.

There will be little discussion of speech recognition and natural language understanding in this paper. Our work focuses solely on recognizing and using nonverbal communicative acts. However, it is well known that gesture and facial expression are intimately tied to speech [14], [38] and one might object to our omission. Nevertheless, our models are theoretically well grounded and models of the same type have been used extensively in speech recognition [45] and dialogue management [41], [57]. Therefore, we believe that our models are ideally suited for integration with dialogue modeling work at some time in the future.

This paper is organized as follows: We first review previous work in modeling human behaviors from both labeled and unlabeled data. Section 3 then describes a general POMDP model of human behavior modeling within a task and Section 4 goes into more detail of a specific POMDP model. Finally, Section 5 discusses the results of learning the model in three situations.

2 Previous Work

Learning and solving POMDPs is a well-studied problem in the artificial intelligence literature. One of the main areas of research is into learning, solving, and using a POMDP simultaneously, online, using reinforcement learning [52]. Although these approaches carry optimality guarantees, they do not scale well to real-world domains. On the other hand, recent developments in efficient approximate solution techniques for specific POMDPs (where the model is known) have shown promise for solving large, realistic problems [9], [29], [50]. However, these methods do not approach the problem of learning the models and typically assume that sensing yields simple observations that are easily quantified. This is a problem in domains that require interactions with humans as the inputs to the decision maker will be very complex. For example, if human facial expressions need to be distinguished for performance in some task, then the observations will be entire sequences of video. Therefore, the decision making process needs to be coupled with some hierarchical modeling that takes care of spatio-temporally abstracting these complex observations. This problem is well studied in computer vision [7], [11], [12], [40], [51], where the goal is to train a classifier to recognize some predefined set of behaviors using supervised learning. Our work instead addresses the coupling between the behavior models and the decision making process: We automatically learn which behaviors are important to recognize.

Representation of human behavior in video is usually done by first estimating some quantity of interest at the pixel level and then spatially abstracting this to a low-dimensional feature vector. Optical flow [6], [20], [21], color blobs [12], [17], deformable models [35], motion energy [7], and filtered images [2] are the more well-used pixel-level features. Spatial abstraction is usually approached using either a model-based or a view-based representation of a body part. Model-based approaches are often three-dimensional wire-frame models [2], sometimes including musculature [21]. View-based approaches spatially abstract video frames by projecting them to a low-dimensional subspace, using, for example, principal components [6], [23], [56], Fisher linear discriminants [3], or independent component analysis [2]. Other representations of faces and bodies use templates [7], feature points [35], or "blobs" [12], [51].

Our work uses Zernike basis functions [44] for holistic representation of the face and facial motion. The Zernike polynomial basis provides a rich and data independent description of optical flow fields and gray-scale images. When applied to optical flow, the Zernike basis can be seen as an extension of the standard affine basis [27]. The Zernike representation differs from approaches such as Eigen-analysis [56], or facial action unit recognition [55] in that it makes no commitment to a particular type of motion, leading to a transportable classification system (e.g., usable for clustering different types of behaviors), which is necessary for a general modeling technique such as we are pursuing. Zernike polynomials have been used for recognizing hand poses [32], handwriting and silhouettes [53], and optical flow fields [28]. It is important to note, however, that our learning method does not rely on this particular choice of basis function and others could be investigated within the same method.

Once features are computed for each frame, their temporal progression must be modeled. Spatio-temporal templates [21], dynamic time warping [18], and hidden Markov models [51] are popular approaches. HMMs have been applied to many recognition problems in computer vision, such as hand gestures [47], American Sign Language [51], and facial action units [2].

There are many DBN extensions of HMMs, including the coupled hidden Markov model [11]. Hierarchical models [22] are particularly interesting as they incorporate temporal abstractions and have been used for modeling full body motions [12]. However, learning a hierarchy is a notoriously difficult problem. *Seer* [40] implements a real-time hierarchical model using a layered HMM, where each layer represents events at a different temporal granularity. However, in *Seer*, each layer is trained independently from labeled data. The DBN underlying a POMDP is known as the input-output hidden Markov model [5]. POMDPs have

been used in realistic domains, including robot control [54] and spoken dialogue management [57]. Darrell and Pentland used POMDPs for control of an active camera [17]. Their POMDP model was trained to foveate regions containing information of interest, such as hands during gesturing. However, their work is focused on computing policies in a reinforcement learning setting. They do not learn the number of behaviors and they separate visual recognition from decision making.

Most of the methods we have been describing are trained with labeled data, which requires human intervention and makes adaptivity more difficult. The alternative is to develop systems that can *discover* categories of motions. In particular, clustering sequences of data using mixtures of hidden Markov models was proposed by Smyth [49] and has been used in computer vision for unsupervised clustering of data [16], [36]. Darrell et al. [18] examine the same kind of models, but use dynamic time warping (DTW). Brand et al. have shown how to discover patterns of motion in an office environment using a hidden Markov model [10], but without hierarchical structure. These works do not explicitly model actions and utilities. Work in human-computer interaction (HCI) has made steps in the direction of learning user behaviors as they relate to system actions. Although most HCI systems only make use of human interface actions, such as mouse or keyboard actions, some have begun to integrate visual and auditory information [42].

Jebara and Pentland [33] presented *action-reaction learning*, in which a dynamic model was learned from observing video of two people interacting. The model was then used in a reactive way to simulate interactions. Our work generalizes action-reaction learning by adding high-level context, actions, and utilities. Action-reaction learning is designed for *imitation*-type tasks, while our model is applicable to interactions in which plans need to be developed autonomously.

3 Learning and Solving POMDPs

A partially observable Markov decision process (POMDP) is a probabilistic temporal model of an agent interacting with the environment. POMDPs can be learned from data, and, once specified, can be used to compute policies of action that maximize some notion of utility. In this section, we first give an overview of POMDPs in Section 3.1, followed by a discussion in Section 3.2 of how to learn the parameters of a POMDP from data with the expectation-maximization algorithm. We show in Section 3.3 how to approximately solve the POMDP by solving the associated MDP model. The solution to the POMDP gives indications about the structure of the model and about how useful this structure is for achieving value.

In this paper, we use standard notation for variables, where capital letters denote random variables, while small letters denote an instantiation of that variable. Subscripts on small letters denote a particular value of a variable. Bold-faced letters represent sets of variables, usually referring to sets that extend over time (e.g., sequences of data). Thus, $\mathbf{X} = \{X_1, \ldots, X_N\}$ is a set of N random variables, $\mathbf{x} = \{x_1, \ldots, x_N\}$ is an assignment of values to those variables, and x_i is an assignment to X_i. We will also write $x_{i,j}$ as the particular assignment $X_i = j$.

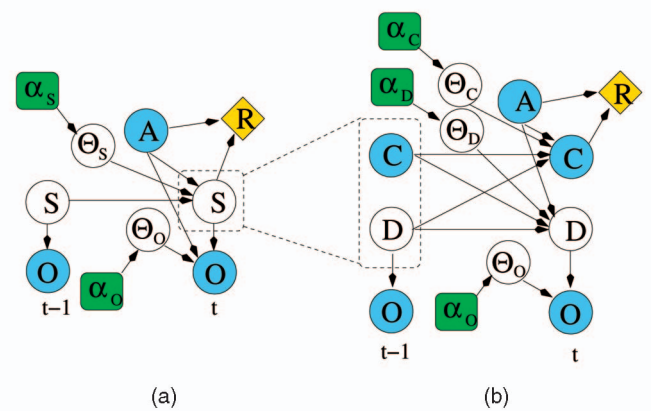

Fig. 1. (a) Two time slices of general POMDP as a dynamic Bayesian network (DBN). (b) The same POMDP with a factored state $S = \{D, C\}$, for display understanding, where D is the unobserved behavior descriptor and C is the remainder of the state, assumed to be fully observable in this paper.

3.1 Overview

A POMDP is a tuple $\langle S, A, \Theta_S, R, O, \Theta_O \rangle$, where S is a finite set of (possibly unobservable) states of the environment, A is a finite set of agent actions, $\Theta_S : S \times A \rightarrow S$ is a transition function that describes the effects of agent actions upon the world states, $R : S \times A \rightarrow \mathbb{R}$ is a reward function that gives the expected reward for taking action A in state S, O is a set of observations, and $\Theta_O : S \times A \rightarrow O$ is an observation function that gives the probability of observations in each state-action pair. Fig. 1a shows two time slices of a POMDP as a dynamic Bayesian network (DBN). Shaded nodes denote observables, unshaded nodes denote unobservable variables. Parameter random variables are denoted by Θ, prior hyperparameters by α, and the diamond is the reward.

When POMDPs are used by a decision maker interacting with another agent (possibly a human), then the state, S, includes some descriptions of the behaviors of this other agent. That is, we factor the state, S, into two parts, $S = \{C, D\}$, as shown in Fig. 1b.[1] Now, D is a high-level description of the observed behaviors of other agent(s), while C contains the remainder of the state, including observable action(s) of the other agent(s). In order to focus on learning models of behaviors, we assume that only D in this model is unobservable directly, while C and A are always fully observed. The transition function is also factorized in two parts: $\Theta_C = P(C_t | C_{t-1}, D_{t-1}, A_t)$ gives the state dynamics given the observed behaviors and the action taken, while $\Theta_D = P(D_t | D_{t-1}, C_t, A_t)$ gives the expected behaviors given the state and action. We assume that C and D are discrete random variables, so the associated parameters Θ_C and Θ_D are multinomial distributions. We denote the complete set of parameters $\boldsymbol{\Theta} = \{\Theta_C, \Theta_D, \Theta_O\}$. We also include fixed prior hyperparameters in Fig. 1: α_C, α_D are Dirichlet prior parameters, while α_O is a more complex prior explored in detail in Section 4.

The observations at time step t, $\mathbf{O}_t$, are a sequence of T_t observations (e.g., video frames), $o_1 \ldots o_{T_t}$. In domains with human behaviors as observations, the rate at which decisions are made at the high level is slower than the rate of

1. Factored representations write the state space implicitly as the cross product of a set of multinomial, discrete variables, and allow conditional independencies in the transition function, T, to be exploited by solution techniques [9].

observations (the video frame rate) and, therefore, $T_t \gg 1$. This difference in temporal scales between decision making and observations means that the observation function must be capable of spatio-temporally abstracting a video stream into a set of high level descriptors of behaviors, D. That is, it must be capable of computing $P(\mathbf{O}_t|D_t)$ and of computing the gradient of this function. We describe one particular such function in Section 4. We assume throughout this paper that the boundaries of the observation sequences will be given by the changes in the fully observable context state, C and A. There are other approaches to the temporal segmentation problem, ranging from the complete Bayesian solution in which the segmentation is parameterized [22] to specification of a fixed segmentation time [40].

A complete set of POMDP parameters, θ, allows us to compute the likelihood of a sequence of data, $\mathbf{o} = \{\mathbf{o}, \mathbf{c}, \mathbf{a}\}$, $P(\mathbf{o}, \mathbf{c}, \mathbf{a}|\theta)$, by summing over the unobserved values of $\mathbf{d}$ using the standard forward algorithm for input-output hidden Markov models [5], [39]. Denoting T as the number of POMDP transitions in the sequence, then $\mathbf{a} = a_1, \ldots, a_T$ and $\mathbf{c} = c_1, \ldots, c_T$ are the *inputs*, $\mathbf{o} = \mathbf{o}_1, \ldots, \mathbf{o}_T$ (where each $\mathbf{o}_t$ is a sequence of video frames) are the *outputs*.

3.2 Learning POMDP Parameters

This section describes how to learn the parameters of a POMDP, which can be formulated as a constrained optimization of the likelihood of the observations, given the model, over the (constrained) model parameters. We will show how the *expectation-maximization*, or EM, algorithm can be used to find a locally optimal solution [19]. Learning takes place over the entire model simultaneously: Both the output distributions, Θ_O, and the high-level POMDP transition functions, Θ_C, Θ_D, are learned from data during the process. Since the behaviors, D, are unobservable, this means that the learning will perform both clustering of the observation sequences into a set of behavior descriptors, D, and learning of the relationship between these behavior descriptors, the observable context, C, and the action, A. In this section, we discuss the general learning method. Section 4.4 shows how to learn the parameters of a hierarchical observation function.

Learning the POMDP parameters is to find the set of parameters, $\boldsymbol{\Theta} = \theta^*$ that maximize the posterior density of all observations and the model, $P(\mathbf{o}, \mathbf{c}, \mathbf{a}, \boldsymbol{\Theta})$, subject to constraints on the parameters. The EM algorithm starts from an estimate of the parameter values, θ', and computes

$$\theta^* = \arg\max_{\boldsymbol{\Theta}=\boldsymbol{\theta}} \left[\sum_{\mathbf{D}=\mathbf{d}} P(\mathbf{d}|\mathbf{o}, \mathbf{c}, \mathbf{a}, \theta') \log P(\mathbf{d}, \mathbf{o}, \mathbf{c}, \mathbf{a}|\theta) + \log P(\theta) \right].$$

The "E" step of the EM algorithm is to compute expectation over the hidden state, $P(\mathbf{d}|\mathbf{o}, \mathbf{c}, \mathbf{a}, \theta')$, given the observations $\mathbf{o}, \mathbf{c}, \mathbf{a}$ and a current guess of the parameter values, θ'. The "M" step is then to perform the maximization which, in this case, can be computed analytically by taking derivatives with respect to each parameter, setting to zero, and solving for the parameter. The resulting update equations for the parameters of the POMDP transition functions are the same as for an *input-output* hidden Markov model [5].

The update equation for the D transition parameter, $\theta_{Dijkl} = P(d_{t,i}|d_{t-1,j}, c_{t,k}, a_{t,l})$, is then

$$\theta_{Dijkl} = \frac{\alpha_{Dijkl} + \sum_{t\in\{1\ldots N_t\}|C_t=k\wedge A_t=l} P(d_{t,i}, d_{t-1,j}|\mathbf{o}, \mathbf{a}, \mathbf{c}, \theta')}{\sum_i \left[\alpha_{Dijkl} + \sum_{t\in\{1\ldots N_t\}|C_t=k\wedge A_t=l} P(d_{t,i}d_{t-1,j}|\mathbf{o}, \mathbf{a}, \mathbf{c}, \theta') \right]},$$

where the sum over the temporal sequence is only over time steps in which the observed values of c_t and a_t in the data are k and l, respectively, and α_{Dijkl} is the parameter of the Dirichlet smoothing prior. The summand can be factored as

$$P(d_{t,i}, d_{t-1,j}|\mathbf{o}, \mathbf{a}, \mathbf{c}, \theta') = \beta_{t,i} P(c_t|d_{t-1,j}, c_{t-1}, a_t) P(\mathbf{o}_t|d_{t,i}) P(d_{t,i}|d_{t-1,j}, c_{t-1}, a_t) \alpha_{t-1,j},$$

where $P(\mathbf{o}_t|d_{t,i})$ is the likelihood of the data given the behavior and α, β are the usual forward and backward variables,

$$\alpha_{t,j} = P(d_{t,j}\mathbf{o}_1, \ldots, \mathbf{o}_t, a_1, \ldots, a_t, c_1, \ldots, c_t),$$
$$\beta_{t,i} = P(\mathbf{o}_{t+1}, \ldots, \mathbf{o}_T, a_{t+1}, \ldots, a_T, c_{t+1}, \ldots, c_T|d_{t,i}, c_t),$$

for which we can derive recursive updates

$$\alpha_{t,j} = \sum_k P(\mathbf{o}_t|d_{t,j}) P(c_t|d_{t-1,k}, c_{t-1}, a_t) P(d_{t,j}|d_{t-1,k}, c_{t-1}, a_t) \alpha_{t-1,k}, \quad (1)$$

$$\beta_{t-1,i} = \sum_k \beta_{t,k} P(c_t|d_{t-1,i}, c_{t-1}, a_t) P(\mathbf{o}_t|d_{t,k}) P(d_{t,k}|d_{t-1,i}, c_{t-1}, a_t). \quad (2)$$

The updates to $\theta_{Cijkl} = P(c_{t,i}|c_{t-1,j}, d_{t-1,k}, a_{t,l})$ are

$$\theta_{Cijkl} = \sum_{t\in\{1\ldots N_t\}|C_t=i\wedge C_{t-1}=j\wedge A_t=l} \xi_k,$$

where $\xi_k = P(d_{t,k}|\mathbf{o}, \mathbf{a}, \mathbf{c}) = \beta_{t,k}\alpha_{t,k}$.

The updates to the jth component of the mixture of the output distributions, $P(\mathbf{O}|D_j)$, will depend on the particular form of that function, but will be weighted by ξ_j. Here, we assume only that the gradient of the observation function can be computed with respect to its parameters. We show more details of these updates in Section 4 for the hierarchical function we have used.

3.3 Solving POMDPs

This section discusses how to solve the learned model to yield a policy of action. If observations are drawn from a finite set, then an optimal policy of action can be computed for a POMDP using dynamic programming over the space of the agent's belief about the state, $b(s)$. Dynamic programming "backs up" the reward function through the POMDP dynamics, thereby computing a value function over the belief space. This value function gives the expected value of the agent being in each belief state and can be used to map belief states into the actions that will achieve this value. Since the belief space is infinite, computing the optimal value function is possible only for very small problems. If the observation space is continuous or very large, as in our case, the difficulty is increased even further [29].

Although the ultimate goal of computing the value function is to yield a policy of action, we are concerned in this paper with *learning* the POMDP model. As we will describe in the next section, the value function has an important role to play in the learning because it gives information about which distinctions in the state space are

useful to make. The ability of the value function to provide this information is intimately connected with its final ability to choose correct actions. However, we can use the simplest possible approximation for a particular domain that still yields sufficient information to guide our learning process. In the domains we have investigated, we can consider the POMDP as a fully observable MDP (the *MDP approximation*): The state, S, is assigned its most likely value in the belief state, $s^* = \arg\max_s b(s)$. Solving the resulting fully observable MDP using dynamic programming consists of computing value functions, V^n, where $V^n(s)$ gives the expected value of being in state s with a *horizon* of n stages to go, assuming optimal actions at each step. The actions that maximize V^n are the policy with n stages to go. The value functions are computed by setting $V^0 = R$ (the reward function), and iterating [4]

$$V^{n+1}(s) = R(s) + \max_{A=a}\left\{\sum_{S=s'} Pr(s'|a,s)\cdot V^n(s')\right\}, \quad (3)$$

where $Pr(s'|a,s)$ is the transition function from s to s' on action a. The actions that maximize (3) form the optimal (with regard to the MDP) n stage-to-go policy, $\pi^n(s)$. We will only consider finite horizon policies in this paper. We use the SPUDD MDP solver, which exploits the structure inherent in a factored representation for efficient solutions [31].

We again stress the fact that, although we are solving the model using a strong approximation, the full POMDP model is still being learned and the solution is only being used in this work to guide our structure learning. For the domains we consider in this paper, this approximation still preserves the information about the state space distinctions necessary to learn the smallest model. It is also important to note that the solution technique we describe here could be replaced with other approximate model-based POMDP solution algorithms. The resulting changes to the value-directed structure learning technique would not alter the basic premise: that state space distinctions which are not useful will be apparent in any reasonable approximate solution.

3.4 Value-Directed Structure Learning

The value function, $V(s)$, gives the expected value for the decision maker in each state. However, there may be parts of the state space that are indistinguishable (or nearly so) insofar as decisions go. Eliminating the distinctions between them by merging states can lead to efficiency gains without compromising decision quality. Such state merging is a form of structure learning (for model order) based upon the utility of states. While this idea has been explored in the machine learning literature [15], we apply it here to the task of learning the minimum number of behaviors that need to be distinguished in our learned POMDP. This *value-directed* structure learning can be contrasted with data-dependent structure learning, in which the complexity of the model is traded off against the quality of fit to the data. For example, Bayesian inference gives rise to a manifestation of Occam's razor by assigning higher probability to simpler models in many cases. However, this only considers utility based on data prediction. In our case, we explicitly look for models that are the simplest for achieving value within a task and these may not be the same as those given by Bayesian model selection.

There are two problems that must be solved: first, finding the parts of the state space that can be merged and, second, actually performing the merging, which involves combining the (learned) observation functions for different behaviors. We address each of these in turn. To merge states, we use the fact that parts of the state space with similar values in the value function can be *aggregated* to form abstract states when computing a policy without sacrificing much in terms of value. We can also look at the policy for a given model and find states that map to the same action. This process is repeated until no more merges are possible or until the number of behaviors becomes 1 (in which case, recognition of the behaviors is deemed useless).

```
initialise N_d as large as possible
repeat
  1.learn the POMDP model
  2.compute V_i and π_i ∀ i
  3.compute d_ij and p_ij ∀ (i,j), i ≠ j
  4.{i,j} = arg min_{kl}(d_kl ∀{k,l} | p_kl > ω_p)
  5.if d_ij < ω_d ∧ N_d > 1
  6.    merge states i and j
  7.    N_d ← N_d − 1
    end
until N_d stops changing
```

Fig. 2. Value-directed structure learning algorithm.

To see how this is implemented, recall that the state space is represented in a factored POMDP as a product over a set of variables. Therefore, the value function can be split into N_d pieces, V_i, one for each value (behavior class) of the variable $D = d_i$. Each such V_i gives the values of being in any state in which $D = d_i$. A similar split occurs for the policy, yielding subpolicies, π_i, giving the actions to take for each $D = d_i$. The V_i can be compared by computing the difference between them, $d_{ij} = \|V_i - V_j\|$, where $\|X\| \equiv max\{|x| : x \in X\}$ is the supremum norm. This value difference is an indication of how much value will potentially be lost if we merge the states i and j. Two subpolicies, π_i and π_j, are compared by dividing the number of states for which they agree, $n_{ij} = |\pi_i \wedge \pi_j|$, by the size of the state space spanned by all variables except D, written $|S_{-D}|$. This fraction, $p_{ij} = n_{ij}/|S_{-D}|$, is the amount of the state space over which the policies agree. The algorithm shown in Fig. 2 uses these measures, beginning with N_d as large as the training data will support. The thresholds ω_p and ω_d govern how aggressively this method merges states. These parameters are not learned and must be tuned manually. We discuss particular values for these thresholds in Section 5.

Once two states have been found, we must initialize a new POMDP model with one state representing the observation space that both original states did (Step 6). We have used two methods for doing this. In the first, we simply delete one of the two states. We use this method in Sections 5.2 and 5.3.2. This may be dangerous, however, as a large part of the observation space may not be modeled and the next iteration of learning (Step 1) may account for it in unpredictable ways. A more principled method is to reinitialize an observation function $P(O|d_i)$, where d_i is the new merged state based on all the data that was classified into states with $D = d_i \vee d_j$ (the old states to be merged). We use this method in Section 5.3.1.

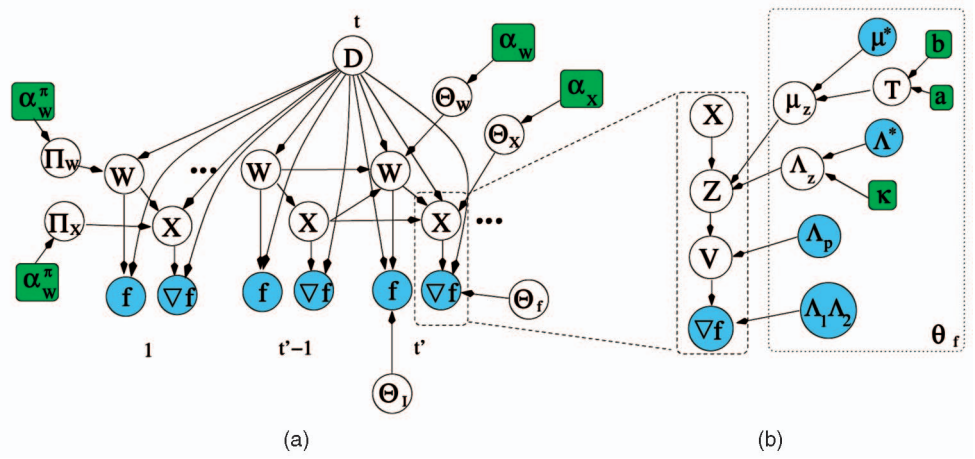

Fig. 3. (a) Two time slices of the hierarchical observation function used in this paper shown as a DBN that parameterizes $P(O|D) = P(f_1 \dots f_{T_l}, \nabla f_1 \dots \nabla f_{T_l}|D)$. Time indices are primed at the low level to distinguish them from the higher level. The low-level time index, t', goes from $1 \dots T$ between times $t-1$ and t at the high level. (b) Bayesian network for the mixture of Gaussians over spatio-temporal image derivatives with feature weighting, parameterizing the distribution $P(\nabla f|X)$ in (a). The distribution $P(f|W)$ is parameterized with a similar network.

4 Observation Function

We now return to the observation function $P(\mathbf{O}|D)$. Recall that this function is a mapping between spatio-temporally extended observations (sequences of video frames), $\mathbf{O}$, and high-level behavior descriptors, D, and, therefore, must have a hierarchical structure. Further, since we will eventually wish to sample from this distribution to find POMDP solutions [29], we require a generative model. Finally, we require that this function be fairly generic such that it can be applied to different types of behaviors without modification. In what follows, we describe a model for $P(\mathbf{O}|D)$ that satisfies all of these constraints, shown as a dynamic Bayesian network in Fig. 3a. It is a mixture of coupled hidden Markov models (CHMMs) [11], a hierarchical dynamic Bayesian network that performs temporal abstraction using hidden Markov chains over X and W. These variables (X, W) describe instantaneous dynamics and configuration of the region being tracked. For example, the configuration classes may correspond to characteristic facial poses, such as the apex of a smile. The dynamics classes are motion classes and may correspond to, for example, motion during expansion of the face to a smile. Section 5.1 shows how configuration and dynamics together outperform either one separately in a recognition task.

We assume that a region of interest in each frame is selected by some independent tracking process (details in [26]). The observations are video image regions, f, and the spatio-temporal derivatives, ∇f, between pairs of images over these regions. The observations are spatially abstracted using projections, Z, to an a priori basis of feature-weighted 2D polynomials, as shown in Fig. 3b. The basis functions are fixed in order to ensure the model is generalizable to different behaviors, but we show in Section 4.3 how feature weights can be learned such that only those basis functions that are necessary are used.

As a generative model, it can be described as follows: A high-level behavior at time t, d_t, generates a sequence of images $f_{t'=1} \dots f_{t'=T}$ and spatio-temporal derivatives, $\nabla f_{t'=1} \dots \nabla f_{t'=T}$ by first generating a sequence of values, $w_{t'=1} \dots w_{t'=T}$ and $x_{t'=1} \dots x_{t'=T}$, for the discrete *configuration* and *dynamics* variables, W and X, respectively. The dynamics in the hidden chains are given by the transition functions $\Theta_X = P(X_{t'}|X_{t'-1}, W_{t'}, D_t)$ and $\Theta_W = P(W_{t'}|W_{t'-1}, X_{t'-1}, D_t)$ and the initialization functions $\Pi_X = P(X_{t'=1}|W_{t'=1}, D_t)$ and $\Pi_W = P(W_{t'=1}|D_t)$. The dynamics and configuration variables at time t', $X_{t'}, W_{t'}$, generate an image, $f_{t'}$ and a spatio-temporal derivative, $\nabla f_{t'}$, through the conditional distributions, $\Theta_I = P(f_{t'}|W_{t'})$ and $\Theta_f = P(\nabla f_{t'}|X_{t'})$. We discuss these last two functions in more detail in Sections 4.1 and 4.2, respectively.

This mixture model can be used to compute the likelihood of a video sequence given the display descriptor, $P(o_1 \dots o_T|d_t)$, where $o_t \equiv \{f_t, \nabla f_t\}$, using the recursive equations:

$$\begin{aligned} P(o_1 \dots o_t|d_t) &= \sum_{ij} P(\nabla f_t|x_{t,i}) P(f_t|w_{t,j}) P(x_{t,i}|x_{t-1,j}, w_{t,k}, d_T) \\ &\quad \sum_{kl} P(w_{t,j}|w_{t-1,k}, x_{t-1,l}, d_T) P(x_{T-1,k}, w_{T-1,l} o_1 \dots o_{T-1}|d_t), \\ p(o_1|d_t) &= \sum_{ij} P(\nabla f_t|x_{1,i}) P(f_t|w_{1,j}) P(x_{1,i}|w_{1,j}, d_t) P(w_{1,j}|d_t). \end{aligned} \tag{4}$$

Table 1 shows the parameters in the model. On the left are parameters that have fixed values. These numbers are set manually based on prior expectations. The right table shows the parameters that are learned using EM, the initialization heuristics, or the value-directed learning methods.

The following sections give more details on the observation function. Sections 4.1 and 4.2 give overviews of the likelihood computations for dynamics, $P(\nabla f_{t'}|X_{t'})$, and configuration, $P(f_{t'}|W_{t'})$, respectively. Feature weighting is described in Section 4.3. Section 4.4 then discusses learning the observation function.

4.1 Dynamics

Fig. 3b shows an expanded version of the dynamics vertical chain from Fig. 3a. We wish to derive the likelihood of a derivative, ∇f, given the high-level dynamics class, X. Since we wish to classify optical flow fields, we expand the likelihood as

TABLE 1
List of Fixed and Learned Parameters in the Model

FIXED

Parameter	Used for	Value
σ_1, σ_2	optical flow	0.08,1.0
$\sigma_{p,x}, \sigma_{p,w}$	projection error	0.01
$N_{z,x}, N_{z,w}$	number of features for X, W	16,32
κ_x, a_x, b_x	feature weights (X)	N_z+2,1,0.01
κ_w, a_w, b_w	feature weights (W)	N_z+2,1,0.01
α_x, α_w	transition priors (X, W)	1.25
$\alpha_x^\pi, \alpha_w^\pi$	initialisation priors (X, W)	1.0
α_D, α_C	transition priors (D,C)	0.1
$\alpha_D^\pi, \alpha_C^\pi$	initialisation priors (D,C)	0.1
N_a, N_c	number of actions, states	
ω_d, ω_p	value-directed thresholds	∞, 0.9

LEARNED

Parameter	Used for	Reference
Θ_D, Θ_C	Transition (D,C)	Sec. III-B
Π_D, Π_C	Initialisation (D,C)	Sec. III-B
N_d	no. states in (D)	Sec. III-D
$\mu_{z,x}, \Lambda_{z,x}, \tau_x$	Mix. of Gaussians (X)	Sec. IV-D
$\mu_{z,w}, \Lambda_{z,w}, \tau_w$	Mix. of Gaussians (W)	Sec. IV-D
Θ_X, Θ_W	Transition (X, W)	Sec. IV-D
Π_X, Π_W	Initialisation (X, W)	Sec. IV-D
N_x, N_w	no. states (X, W)	Sec. IV-D

$$P(\nabla f|X,\Theta) = \int_v P(\nabla f|v,\Theta)P(v|X,\Theta), \tag{5}$$

where we have assumed the derivatives independent of the motion class given the flow, v.

There are two terms in the integration. The distribution over spatio-temporal derivatives conditioned on the flow, $P(\nabla f|v,\Theta)$, is estimated in a gradient-based formulation using the brightness constancy assumption and is given by:[2] $P(\nabla f|v) \propto \mathcal{N}(f_\tau; -f_s v, A)$, where $A = f_s \Lambda_1 f_s' + \Lambda_2$, and Λ_1, Λ_2 are noise covariances in the optical flow estimation [48]. $P(v|X)$ is parameterized using a projection of v to the basis of Zernike polynomials, $P(v|X) = \int_{z_X} P(v|z_X)P(z_X|X)$, where Z_X is the feature vector in the polynomial basis space. We parameterize the distribution over Z_X given X with a normal, $P(Z_X|X) = \mathcal{N}(Z_X; \mu_{z,x}, \Lambda_{z,x})$. We are expecting flow fields to be normally distributed in the space of the basis function projections.

The distribution over v given z_X is given by projections to the basis of Zernike polynomials, which have useful properties for modeling flow fields [27] and images [53]. Our method is not restricted to this basis set, but gains independence from the data by using an a priori set of basis functions, leading to a more generally applicable observation function. Zernike polynomials are an orthogonal set of complex polynomials defined on a 2D elliptical region as follows [44]:

$$\begin{bmatrix} A_n^m(x,y) \\ B_n^m(x,y) \end{bmatrix} = \sum_{l=0}^{(n-|m|)/2} \frac{(-1)^l (n-l)!}{l!\left[\frac{1}{2}(n+|m|)-l\right]!\left[\frac{1}{2}(n-|m|)-l\right]!\rho^{n-2l}} \begin{bmatrix} cos(m\phi) \\ sin(m\phi) \end{bmatrix}, \tag{6}$$

where $\phi = \arctan(y/x)$, $\rho = \sqrt{x^2+y^2} \leq 1$, and x, y are measured from the region center. The lowest two orders of Zernike polynomials correspond to the standard affine basis, and higher orders (higher values of n and m) represent higher spatial frequencies. The basis is orthogonal such that each order can be used as an independent characterization of a 2D function and each such function has a unique decomposition in the basis. Define an $N \times N_z$ matrix B whose columns are the N_z Zernike basis functions (with pixels arranged rowwise), alternating between A_n^m and B_n^m such that columns $0, 1, 2, 3 \ldots$ are Zernike polynomials $A_0^0, A_1^1, B_1^1, A_0^2 \ldots$. Then, a 2D function, f, with N pixels is projected to the basis using $z = \epsilon B' f$ and can be reconstructed from the $N_z \times 1$ column vector of coefficients, z, using $f = Bz$. The normalization constant $\epsilon = \epsilon_m(n+1)/\pi$, where $\epsilon_m = 1$ if $m = 0$ and $\epsilon_m = 2$ otherwise. Each of the vertical and horizontal components of a flow field can be written as a linear combination of the basis functions and, so, we can write $v = Mz_X$, where

$$v = \begin{bmatrix} v_x \\ v_y \end{bmatrix} \quad M = \begin{bmatrix} B & 0 \\ 0 & B \end{bmatrix} \quad z_X = \begin{bmatrix} z_x \\ z_y \end{bmatrix}, \tag{7}$$

in which z_x, z_y are the Zernike coefficients for horizontal and vertical flow, respectively. In practice, M will be some subset of the Zernike basis vectors, the remaining variance in the flow fields being attributed to zero-mean Gaussian noise. Thus, we write $v = Mz_X + n_p$, where $n_p \propto \mathcal{N}(0, \Lambda_p)$ and, so, $P(v|z) = \mathcal{N}(v; Mz_X, \Lambda_p)$. The noise, n_p, is a combination of three noise sources: the reconstruction error (energy in the higher order moments not in M), the geometric error (due to discretization of a circular region), and the numerical error (from discrete integration) [37]. The choice of a subset of basis elements to use will depend on what the projections are being used for (see Section 4.3).

Since all of the terms in the integration (5) are Gaussian distributions, we can integrate over v and z analytically by successively completing the squares in v and z_X to obtain

$$P(f_\tau|Xf_s) = \frac{\sqrt{|\tilde{\Lambda}_{z,x}|}}{\sqrt{|A||\Lambda_{z,x}|}} e^{\frac{1}{2}(\tilde{\mu}_{z,x}' \tilde{\Lambda}_{z,x}^{-1} \tilde{\mu}_{z,x} - \mu_{z,x}' \Lambda_{z,x}^{-1} \mu_{z,x} - \epsilon)}, \tag{8}$$

2. The spatio-temporal derivative is $\nabla f = \{f_s, f_\tau\}$, where $f_s = \{f_x, f_y\}$ is the spatial derivative and f_τ is the temporal derivative. The expression $f_s v$ means $f_x v_x + f_y v_y$, where v_x, v_y are the horizontal and vertical optical flow field, respectively.

where

$$\begin{aligned}\tilde{\Lambda}_{z,x} &= \left(\Lambda_{z,x}^{-1} + M'\left(\Lambda_p + \left(f_s' A^{-1} f_s\right)^{-1}\right)^{-1} M\right)^{-1},\\ \tilde{\mu}_{z,x} &= \tilde{\Lambda}_{z,x}\left(\Lambda_{z,x}^{-1}\mu_{z,x} - M'\Lambda_p^{-1}\Lambda_w w\right),\\ \Lambda_w &= \left(f_s' A^{-1} f_s + \Lambda_p^{-1}\right)^{-1},\\ \epsilon &= f_\tau' A^{-1} f_\tau + w'\Lambda_w w \;\; w = f_s' A^{-1} f_\tau.\end{aligned} \tag{9}$$

The brightness constancy assumption fails if the velocity v is large enough to produce aliasing. Therefore, a multiscale pyramid decomposition of the optical flow field must be used. This results in distribution over the flow vectors, $P(v|\nabla f) \sim \mathcal{N}(v; \mu_v, \Lambda_v)$, where $\Lambda_v = (f_s' A^{-1} f_s)^{-1}$ and $\mu_v = -\Lambda_v f_s' A^{-1} f_\tau$ [48]. Using these coarse-to-fine estimates, (9) become

$$\begin{aligned}\tilde{\Lambda}_{z,x} &= \left(\Lambda_{z,x}^{-1} + M'(\Lambda_p + \Lambda_v)^{-1} M\right)^{-1},\\ \tilde{\mu}_{z,x} &= \tilde{\Lambda}_{z,x}\left(\Lambda_{z,x}^{-1}\mu_{z,x} + M'(\Lambda_p + \Lambda_v)^{-1}\mu_v\right).\end{aligned} \tag{10}$$

The mean of this distribution, $\tilde{\mu}_{z,x}$, is a weighted combination of the mean Zernike projection from the data ($M'\mu_v$) and the model mean, $\mu_{z,x}$.

4.2 Configuration

The classification of image configurations proceeds analogously to the classification of temporal derivatives. We use the same set of basis functions, but the measurements are now the images, I, the subspace projections over image regions are H and the basis feature vectors are Z_W. The distribution over Z_W given W is parameterized with a normal $P(Z_W|W) = \mathcal{N}(Z_W; \mu_{z,w}, \Lambda_{z,w})$. The distribution over the image regions given the Zernike projection is normal, $P(H|Z_W, \Theta) = \mathcal{N}(H; BZ_W, \Lambda_q)$. The distribution over images given the subspace image region, h, $P(f|H, \Theta)$, can be approximated using a normal distribution at each pixel, $P(f|H, \Theta) \sim \mathcal{N}(f; H, \Lambda_h)$.

The integrations give results similar to that for the dynamics (8):

$$P(f|W, \Theta) \propto e^{\mu_\diamond' \Lambda_\diamond^{-1}\mu_\diamond - \mu_{z,w}'\Lambda_{z,w}^{-1}\mu_{z,w}}, \tag{11}$$

where

$$\begin{aligned}\mu_\diamond &= \Lambda_q^{-1}\left[\Lambda_h^{-1} + \Lambda_q^{-1}\right]^{-1}\Lambda_h^{-1} f' + \Lambda_{z,w}^{-1}\mu_{z,w},\\ \Lambda_\diamond &= \left(B'\Lambda_q^{-1}B - B'\Lambda_q^{-1}\left[\Lambda_h^{-1} + \Lambda_q^{-1}\right]^{-1}\Lambda_q^{-1}B - \Lambda_{z,w}^{-1}\right)^{-1}.\end{aligned}$$

In this case, however, there are no data-dependent variances and we approximate $P(f|W\Theta) = P(z_W|W\Theta)$, where $z_W = B'f$ is the projection of the image region to the basis.

4.3 Feature Weighting

In general, we will not know which basis coefficients are the most useful for our classification task: which basis vectors should be included in M and which should be left out (as part of n_p). We use the feature weighting techniques of [13] that characterize the relevance of basis vectors by examining how the cluster means,[3] μ_z, are distributed along each basis dimension, $k = 1 \ldots N_z$. Relevant dimensions will have well-separated means (large interclass distance along that dimension), while irrelevant dimensions will have means that are all similar to the mean of the data, μ^*.

To implement these notions, we place a conjugate normal prior on the cluster means, $\mu_z \sim \mathcal{N}(\mu^*, T)$, where T is diagonal with elements $\tau_1^2 \ldots \tau_{N_z}^2$ and τ_k^2 is the feature weight for dimension k. The prior biases the model means to be close to the data mean along dimensions with small feature weights (small variance of the means), but allows them to be far from the data mean along dimensions with large feature weights (large variance of the means). Thus, τ_k^2 will be large if k is a dimension relevant to clustering, while $\tau_k^2 \to 0$ if the dimension is irrelevant. Feature selection occurs if we allow $\tau_k^2 = 0$ for some k. We do not select features in this work.

Conjugate priors are placed on the feature weights, τ_k^2, and on the model covariances, Λ_z. Each feature weight is univariate and, so, an inverse gamma distribution is the prior on each τ_k^2:

$$P(\tau_k^2|a, b) \propto (\tau_k^2)^{-a-1} e^{-b/\tau_k^2}. \tag{12}$$

This prior allows some control over the magnitude of the learned feature weights, τ_k^2. The model covariances are multivariate, for which the conjugate prior is an inverse-Wishart prior:

$$P(\Lambda_z|\alpha, \Lambda^*) \propto |\Lambda_z|^{-(\kappa+N_z+1)/2} e^{-\frac{1}{2}tr(\alpha\Lambda^*\Lambda_z^{-1})}, \tag{13}$$

where Λ^* is the covariance of all the data and κ is a parameter that dictates the expected size of the clusters (the intraclass distance). This prior stabilizes the cluster learning.

4.4 Learning the Observation Function

Recall from Section 3.2 that the updates (M step) to the jth component of the output distribution, $P(O|D_j)$, will be weighted by $P(d_{t,j}|\mathbf{o}, \mathbf{a}, \mathbf{c}) = \alpha_{t,j}\beta_{t,j}$, where α and β are the forward and backward variables ((1) and (2)), respectively, that require the computation of $P(\mathbf{o}|d_{t,j})$ as given by (4). This means that we can use the standard equations for updating the transition functions in the X and W chains as would be used for a normal CHMM, except the evidence from the data is weighted by $P(d_{t,k}|\mathbf{o}, \mathbf{a}, \mathbf{c})$.

The updates to the output distributions in the configuration process, $P(f|W)$, and in the dynamics process, $P(\nabla f|X)$, are as they would be in a mixture model, except that the feature weights bias the updates toward the prior distributions, and the prior weights are given by the state likelihoods in the POMDP (high-level) chain. The update equation for the mean of the ith Gaussian output distribution in the jth model (a component of $P(\mathbf{o}|x_{t,i}, d_{t,j})$), $\mu_{z,ij}$, is

$$\mu_{z,ij} = (\xi_{\cdot,ij}\Lambda_{z,ij}^{-1} + T_j^{-1})^{-1}\left[\Lambda_{z,ij}^{-1}\left(\sum_{t'=1}^{T_t}\tilde{\mu}_{z,xij}\xi_{t',ij}\right) + T_j^{-1}\mu^*\right],$$

where $\xi_{\cdot,ij} = \sum_{t'=1}^{T_t}\xi_{t',ij}$, $\tilde{\mu}_{z,xij}$ is given by (10) using the parameters of the ith Gaussian output in the jth model, $\mu_{z,xij}, \Lambda_{z,xij}$, and

$$\begin{aligned}\xi_{t',ij} &= P(x_{t',i}d_{t,j}|\mathbf{o}, \mathbf{a}, \mathbf{c}\theta')\\ &= P(x_{t',i}|o_{t'=1} \ldots o_{t'=T}, d_{t,j}, \theta')P(d_{t,j}|\mathbf{o}, \mathbf{a}, \mathbf{c}, \theta').\end{aligned}$$

The first term is given by the the usual forward-backward equations in a CHMM [11], while the second is given by the forward-backward equations in the high-level POMDP ((1) and (2)). Thus, the most likely mean for each state x is the weighted sum of the most likely values of z as given by (10).

3. We drop the subscript x or w here since these equations apply equally to the X or W output distributions.

Dimensions of the means, $\mu_{z,i}$, with small feature weights, τ_k^2, will be biased toward the data mean, μ^*, in that dimension. This is reasonable because such dimensions are not relevant for clustering and, so, should be the same for any cluster, X.

The updates to the feature weights are

$$\tau_k^2 = \frac{b}{a + N_x/2 + 1} + \frac{1}{2a + N_x + 2} \sum_{i=1}^{N_x} (\mu_{z,i,k} - \mu_k^*)^2$$

and show that those dimensions, k, with $\mu_{z,i,k}$ very different from the data mean, μ_k^*, across all states, will receive large values of τ_k^2, while those with $\mu_{z,i,k} \sim \mu_k^*$ will receive small values of τ_k^2. Intuitively, the dimensions along which the data is well separated (large interclass distance) will be weighted more. The complete derivation, along with the updates to the output distributions of the CHMMs, including to the feature weights, can be found in [26].

Model initialization proceeds in a bottom-up fashion. First, the dynamics mixture model with N_x classes is initialized from a set of single (time-independent) spatio-temporal derivative fields, $\nabla \mathbf{f}$, by first computing the expected most likely values of z_x for each frame using a single zero-mean model with constant diagonal covariance 0.001 and then fitting a Gaussian mixture to the result of K-means clustering with $K = N_x$ [28]. While the K-means algorithm uses the Euclidean distance in the space of Z, the Gaussian fits use the Mahalanobis distance. All of the feature weights, τ_k^2, are initialized to 1 and state assignment probability Θ_X is initialized evenly. The mixture model over the configurations is initialized in a similar way, using the projections of image regions to the Zernike basis.

The entire model is initialized using the estimates of dynamics and configuration mixtures by first classifying all of the data using the two mixture models and finding the largest N_d sets of sequences whose sets of visited X states match exactly. Second, find the set of X (W) states visited by all the sequences in set i: N_X^i (N_W^i). Third, initialize a CHMM for each set, i, by assigning the output distributions to be those in the simple mixture models visited by the sequences in the cluster. The transition and initial state probabilities are initialized randomly. Finally, training each CHMM, keeping the output distributions fixed and initializing the mixture probabilities for the mixture of CHMMs evenly for each context state.

4.5 Complexity

The complexity of parameter learning is dominated by the computation of (10) in the "E" step, which is $O(N_d[N_p N_z + N_z^3]T'')$, where N_d is the number of high-level display states, T'' is the length of the entire sequence of data, N_p is the maximum number of pixels in the region being tracked, and N_z is the maximum dimensionality of the feature vectors Z_x, Z_w. The computation is repeated until EM converges, usually some small number of iterations $n < 10$.

The worst-case complexity of solving the POMDP using value iteration over the associated MDP is $O(N_s^2 N_a H)$, where N_s is the number of states in the POMDP, N_a is the number of actions, and H is the horizon. In typical problems, N_s is very large (exponential in the number of variables in the POMDP) and the complexity of the entire system, learning plus solution, will be dominated by the solution term. In the experiment described in Section 5.3, the number of features is $N_z = 36$ (the major factor in the learning complexity), but the number of states is $N_s > 6 \times 10^5$. Note, however, that we use a structured approach to solving this MDP [31], which can substantially reduce the solution average case complexity.

Once a policy has been found, the complexity of using the model online is composed of updating the belief state ($O(N_o N_s^2)$) and consulting the policy ($O(N_s N_a)$). The belief state inference will dominate for any reasonably sized model, but techniques that leverage structure can substantially reduce the running time so as to make this possible in near real-time. The other major computation is optical flow, which can be done in near-real-time as well.

5 Experiments

We present three sets of experiments in this section, each designed to address a particular issue in the learning method we have presented. In the first (imitation game), we explore the representational power of our computer vision modeling techniques by examining how they can be used to learn fairly complex facial expressions. The second experiment demonstrates the value-directed learning technique using a simple set of hand gesture sequences. The third experiment then shows how the model can be used to learn a more complex interaction during a card matching game. We demonstrate on both synthetic and real data in this third experiment.

5.1 Imitation Game

In this experiment, human subjects imitated the facial expressions of an animated character. We learn a mixture of CHMMs model of their facial expressions and use this model to predict the animation that caused it. To play the imitation game, a player watches a computer animated face on a screen and is told to imitate the actions of the face. The animations start from a neutral face (n) and warp to one of four poses $\{a_1, a_2, a_3, a_4\}$, as shown in Fig. 4. The pose is held for one second and the face then warps back to neutral, where it remains for an another second.

The simplified model is shown in Fig. 4b. The cartoon facial expressions are $A = \{a_1 \ldots a_4\}$, the observations of the human's actions, $\mathbf{O}$, are sequences of video images and the spatio-temporal derivatives between subsequent video frames and the descriptor of the human's facial expression is $D \in \{d_1 \ldots d_{N_d}\}$. The key here is the ability to learn both the output distribution $P(O|D)$ and the relationship between the player's behavior, D, and the cartoon display, A, $P(D|A)$. Thus, we train the model on a set of training data in which the cartoon display labels are observed, then we attempt to predict the cartoon facial expression on a set of test data in which the labels are hidden. That is, on the test data, we compute $a^* = \arg\max_a P(A = a|\mathbf{o}) = \arg\max_a \sum_i \; P(\mathbf{o}|d_i)P(d_i|A = a)$.

Three subjects performed the task 40 times each. Video frames were recorded at 160×120 with a Sony EVI-D30 color camera (framerate 28 fps) mounted above the screen. The subjects' faces were located in each frame using an optical flow and exemplar-based tracker [26]. The videos were temporally segmented using the onset times of the cartoon facial expressions and the resulting sequences were input to the mixture of coupled HMM clustering and training algorithm using four clusters ($N_d = 4$, the number of expressions the subjects were trying to imitate).

We did a leave-one-out cross validation experiment for each of the subjects to verify the prediction accuracy. There were 40 sequences for each subject, one of which was

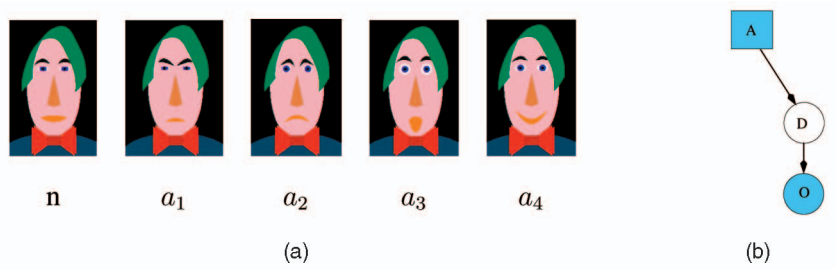

Fig. 4. (a) Cartoon faces: neutral (n) and facial expressions $A = \{a_1 \dots a_4\}$). (b) Graphical model of the imitation game.

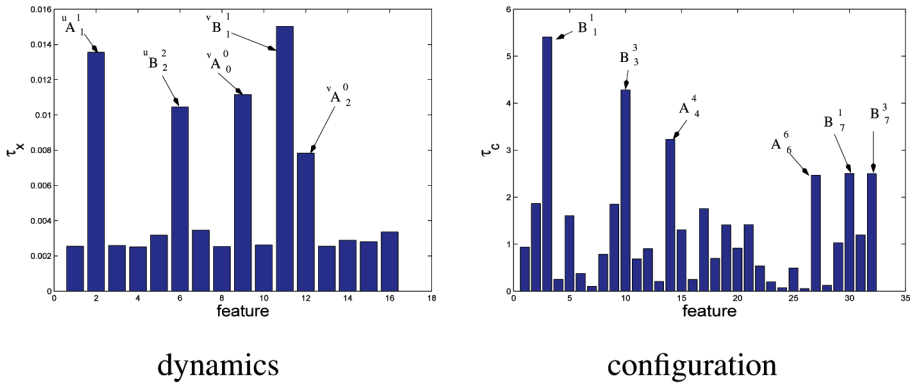

Fig. 5. Feature weights τ_k^2 for model 1 dynamics and configurations chains.

removed. The remaining 39 sequences were used to train the POMDP. The learned model was used to infer A from the remaining sequence (in which it is hidden) and the most likely value was compared to the actual display. This process was repeated for all 40 left-out sequences, giving the best unbiased estimated of performance on the whole set of data. This process was repeated three times for each subject with different random initializations, with average success rates of 78, 74, and 62 percent. However, these results ignore the model's explicit representation of uncertainty, only reporting success if the actual display is the peak of $P(A|\mathbf{O})$. In some cases, there is a second display that is nearly as likely as the best one. The success rates rise to 95, 93, and 84 percent if we count those classifications as correct where the probability of the most likely display is less than 0.5 and the second most likely display is the correct one.

We also used this game to evaluate the modeling of both the dynamics and the configuration in the observation CHMMs. We performed the same leave-one-out experiment on the first subject's data with 10 random intitializations, and for each seed, we trained one model with only dynamics (X) states, one with only configuration (W) states, and one with both. Results showed that modeling both outperformed either separately: 76 percent for both compared to 68 percent for dynamics alone and 68 percent for configuration alone.

We now show some details of thee learned $D = 1$ ("smiling") model for one subject. Feature weights are shown in Fig. 5. The dynamics chain has four significant features: two in the horizontal flow, ${}^{u}A_1^1, {}^{v}B_2^2$, and three in the vertical flow, ${}^{v}A_0^0$, ${}^{v}B_1^1$, and ${}^{v}A_2^0$. The three most significant features in the configuration chain are B_1^1, B_3^3, and A_4^4. The output distributions of the four dynamics states (X) are shown in Fig. 6a, plotted along the two most significant feature dimensions, ${}^{u}A_1^1$ and ${}^{v}B_1^1$. Two states ($X = 2, 4$) correspond to no motion, while the other two correspond to expansion upward and outward in the bottom of the face region ($X = 1$) and contraction downward and inward in the bottom of the face region ($X = 3$). These states correspond to the expansion and relaxation phase of smiling. The output distributions of the four configuration states are shown in Fig. 6b. There are two states ($W = 2$ and $W = 4$) which describe the face in a fairly relaxed pose, while $W = 1$ and $W = 3$ describe "smiling" configurations, as evidenced by the darker patches near the sides at the bottom.

Fig. 7 shows the model's explanation of a sequence in which $D = 1$. We see the high level distribution over D is peaked at $D = 1$. Distributions over dynamics and configuration chains show which state is most likely at each frame. The expected pose, H, and flow field, V, are shown conditioning the image, f, and the temporal derivative, f_t, respectively.

5.2 Robot Control Gestures

This "game" involves a human operator issuing navigation commands to a robot using hand gestures. The robot has four possible actions, A: *go left*, *go right*, *stop*, and *go forward* and the operator uses four hand gestures corresponding to each command. The state, C, is the operator's action: A Boolean indicator of whether the robot took the right action or not. The reward function is 1 if the robot took the correct action ($C = 1$); otherwise, it is 0. It is important to state that these experiments do not demonstrate gesture recognition, but only the value-directed learning. Realistic robotic control requires more complex tracking to deal with moving platforms and the high variability in gestures.

We recorded 12 examples of each of four gestures performed by a single subject in front of a stationary camera. Video was grabbed from a IEEE 1394 (Firewire) camera at 150×150. The region of interest was the entire image, so no tracking was required. Sequences were taken of a fixed length of 90 frames. From the original 12 data sequences, we selected

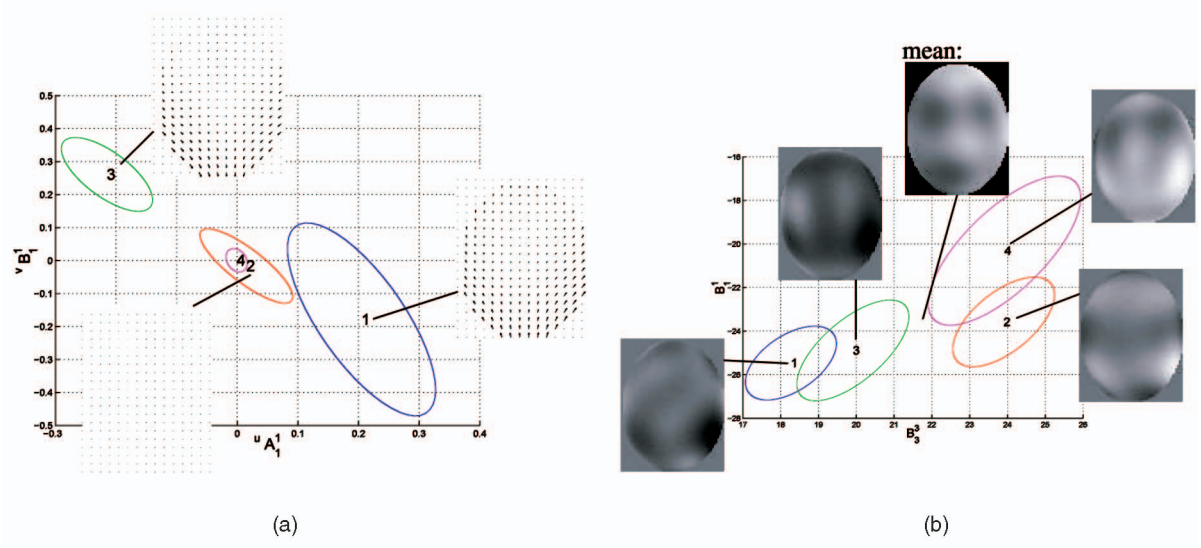

Fig. 6. (a) Dynamics chain model 1 output states plotted along two most significant dimensions according to feature weights, ${}^{u}A_1^1, {}^{v}B_1^1$. Reconstructed flow fields for X state means are also shown. (b) Configuration chain model 1 output distributions. The differences between the W state means and the overall data mean are shown, as well as the overall data mean in the center.

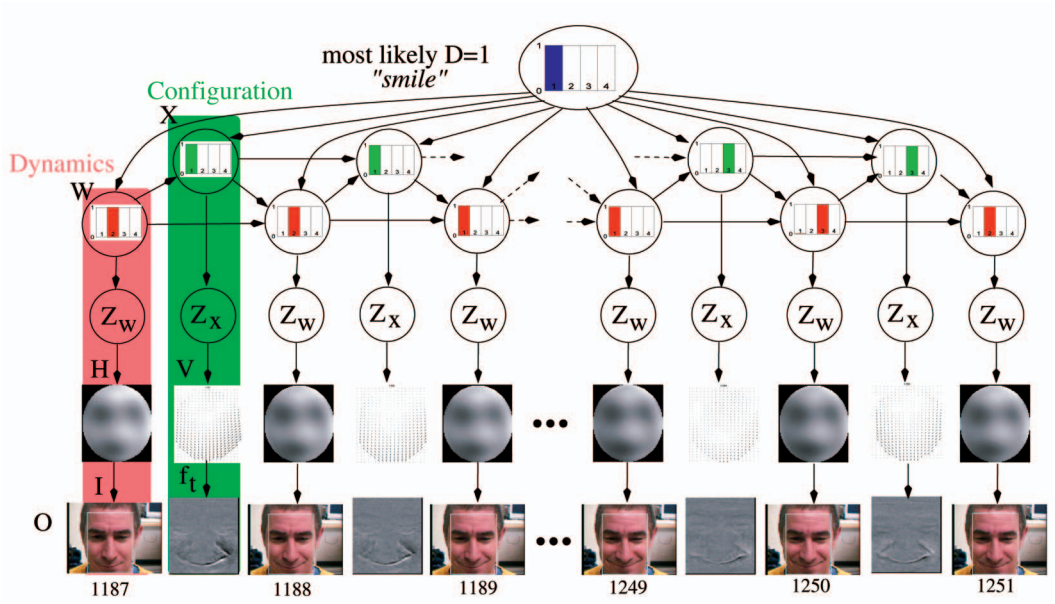

Fig. 7. A person smiling is analyzed by the mixture of CHMMs. Probability distributions over X and W are shown for each time step. All other nodes in the network show their expected value given all evidence.

11 from each gesture and constructed a training set in which each A was tried for each possible gesture sequence (and the resulting C response was simulated), giving a total of 44 training sequences. We used an initial $N_d = 6$ states, which is as many as we can expect to learn given the amount of training data. The value-directed structure learning algorithm used $w_p = 0.9$ and $w_d = \infty$.

Once the model is trained on the 44 training sequences, we evaluate how well it chooses an action on the four remaining sequences (one for each gesture). This leave-one-out cross-validation is repeated for 12 different sets of four test sequences and the total rewards gathered give an unbiased indication of how well the model performs on unseen data. The model chose the correct action 47 out of a total of $12 \times 4 = 48$ times, for a total success rate of 47/48 or 98 percent. The one failure was due to a misclassification of a "left" gesture as a "right" gesture due to a large rightward motion of the hand at the beginning of the stroke. More importantly, the final POMDP models learned that there were $N_a = 4$ states in all 12 cases.

5.3 Card Matching Game

The card matching game is a simple cooperative two-player game in which the players must send signals to each other through a video link in order to win. At the start of a round, each player is dealt three cards: a heart, a diamond, and a spade. Each player can only see his own set of cards. The players must each play a single card simultaneously and, if the suits match, the players win a function of the amount on the cards; otherwise, they incur a fixed penalty. Thus, the goal of the game is to agree on which suit to play to maximize the return. In order to facilitate this, one player (the *bidder*) can send a *bid* to their partner (the *ally*), indicating a card suit, and can see (but not hear) the *ally*

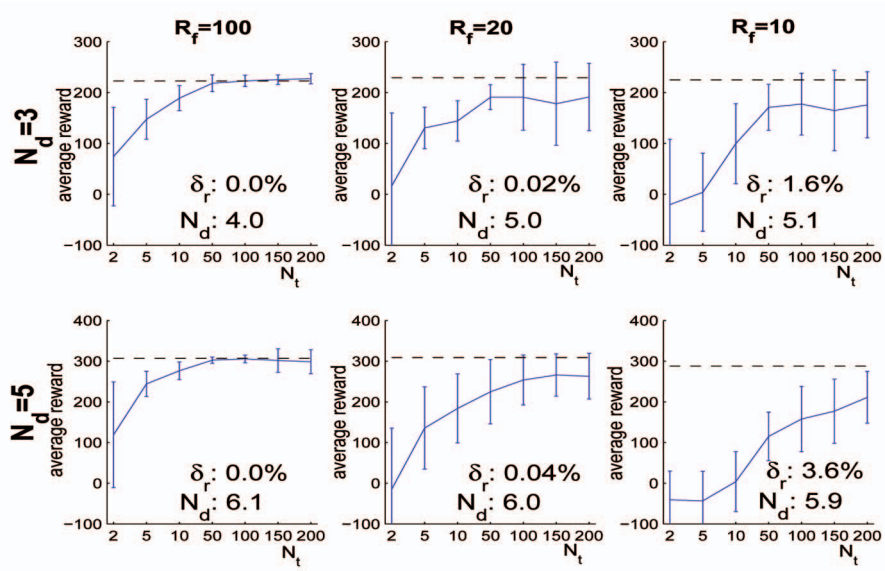

Fig. 8. Average reward gathered over 20 trials in simulation, for simulated models with (top row) $N_d = 3$ and (bottom row) $N_d = 5$ (three and five behaviors to be recognized, respectively), shown as a function of the number of training sequences. The three plots in each row show the results for $R_f = 100$, 20, and 10, from left to right. The dashed line in each plot shows the mean reward achieved when the model is given as the simulated model and, so, is optimal for the given simulation. The values of N_d shown in the plot are the averages learned by the algorithm for $N_t = 200$.

through a real-time video link. Thus, the expectation is that the *ally* will develop a gesturing strategy to indicate agreement with the bid. For example, a simple strategy involving two head gestures is for the ally to nod or shake her head in agreement or disagreement with the bid. A more complex strategy is to develop a set of three head or hand gestures for each card suit. This game is similar to games used in psychology to study the emergence of language [25], [34]. We use it because the number and form of the gestures are not specified as rules of the game, but instead are decided upon by the players at game time.

There are nine variables that describe the state of the game. The suit of each of the three cards can be one of $\heartsuit, \diamondsuit, \clubsuit$. The bidder's actions, A, can be $null$ (no action) or sending a confidential bid ($bid\heartsuit, bid\diamondsuit, bid\clubsuit$) or committing a card ($cmt\heartsuit, cmt\diamondsuit, cmt\clubsuit$). The ally's action, C, can be $null$ or committing a card ($cmt\heartsuit, cmt\diamondsuit, cmt\clubsuit$). The behavior variable, $D = d_1 \ldots d_{N_d}$, describes the ally's communication through the video link. The other six observable variables in the game are more functional for the POMDP, including the values of the cards ($v1, v2$ for bidder and ally, respectively) and whether a match occurred or not. The reward is a function of fully observable variables only and is $(v1 + v2)[1 + (v1 > 1 \wedge v2 > 1)]$ if the suits match and -10 otherwise. The number of display states, N_d, is learned using the value-directed structure learning technique in Fig. 2. The number of states in the MDP is $20,736 N_d$.

5.3.1 Simulated Results

Since our model is generative, we can use it to simulate the game and to generate data. We first specified two prior models for the card matching game: The first, M_1, has $N_d = 3$, while the second, M_2, has $N_d = 5$. We randomly specify a complete set of output distribution parameters, $P(\mathbf{O}|D)$, as follows: Transition matrices were drawn randomly in $[0\ 1]$, but with added weight of 30.0 on the diagonal (followed by a renormalization). Feature weights for all output distributions were drawn randomly in $(0\ R_f]$. The means were drawn from the model priors given these feature weights. Covariance matrices were set to be diagonal with a variance in each dimension of $(10.0 + c)^2$, where c is normally distributed with variance 1.0. We used $N_{z,x} = N_{z,w} = 4$. The parameter R_f varies the "overlap" between output distributions. The larger R_f is, the more distinguishable the behavior models will be. We can estimate the degree of "overlap" of the output distributions by using them to simulate data and then measuring the maximum-likelihood error rates, δ_r, on this data given the models. We used three values of $R_f = \{10, 20, 100\}$, which gave error rates on 50,000 simulated sequences of 1.6, 0.02, and 0.0 percent, respectively, for model M_1, and 3.6, 0.04, and 0.0 percent, respectively, for model M_2.

Once the model was specified, we simulated a set of N_t training sequences from it, each of length $T = 100$, with output sequences of a fixed length of $T' = 20$, using a random selection of actions, A. We only simulate the values of Z_W, Z_X, not the full observation set, $f, \nabla f$, since this is sufficient to demonstrate the method. We then applied the training process in Fig. 2 on these N_t training sequences, using $w_p = 0.6$ and $w_d = 20.0$, and starting with $N_d = 8$. The learned model and policy was tested for 20 trials of length 100 and we record the average reward gathered over the 20 trials. The whole process is repeated (including random specification of new output distributions) 20 times and the means and standard deviations of the averages are recorded. We also estimate the optimal values that can be achieved by performing the same simulation experiment, but using the original simulated model instead of a learned model.

Fig. 8 shows the results. Each plot shows the average reward and standard deviation for each value of N_t, as well as the optimal value (dashed line), the average number of behavior models (for $N_t = 200$), N_d, and the degree of overlap, δ_r. The average number of states of D learned for $N_t = 200, R_f = 100$ was 4.0 and 6.1 for $N_d = 3$ and $N_d = 5$, respectively, showing that, although the state merging was not overly aggressive, it managed to reduce the model order close to that of the true models in both cases. The results show that, if the actual output models are distinguishable

($R_f = 100$), then the resulting learned model is nearly optimal for $N_t \gtrapprox 50$, even using the approximate solution technique for the POMDP policy. This is what we expect to happen if the learning technique is able to recover a set of behaviors that distinguish at least those behaviors that are important to the task, since then the state is (nearly) fully observable and the MDP policy is (nearly) optimal for the POMDP. On the other hand, when the output models become less easily distinguishable (for $R_f = 20$ and 10), the learning is more difficult and, so, the gap between the optimal solution and the learned one widens. Nevertheless, the performance remains close to optimal in all but the most difficult case (with $N_d = 5$ and $R_f = 10$).

5.3.2 Real Data

The card matching game was played by two users through a computer interface in our laboratory. Each player viewed their partner through a link from their workstation to a Sony EVI S-video camera mounted atop their partner's screen. The average frame rate at 320×240 resolution was over 28 fps. The rules were explained to the subjects and they played four games of five rounds each. The players had no chance to discuss strategies before the game, but were given time to practice. The player's faces were tracked using the same tracker as in Section 5.1, described in [26]. In this experiment, the partner used the obvious communication strategy of "nodding" and "shaking" their head in response to good and bad bids, respectively.

The model was trained with four display states, which is as large as we think is possible to learn reliable models given the training set size. The structure learning algorithm was applied with $\omega_p = 0.9$ and $\omega_d = \infty$, which finds values of D for which the subpolicies match over 90 percent of the state space. Two values of D had policies that were in $p_{01} = 0.96$ agreement (96 percent of the state space) and were merged. The result was, as expected, one "null" state (d_1), one "nodding" state (d_2), and one "shaking" state (d_3). No further merges were found. The associated policy correctly predicted 14/20 actions in the training games and 5/7 actions in the test game.

In order to attenuate the effects of the lack of training data, we use symmetry arguments to *fill in* the model without having to explicitly explore those situations. In particular, we may assume that players do not have any particular preference over card suits such that the conditional probability tables should be symmetric under permutation of suits. Therefore, we can "symmeterize" the probability distributions by simply averaging over the six card suit permutations. The policy for the symmetrized POMDP correctly predicts all but one (19/20) action in the training game, for an error rate of 5 percent. The misclassification was due to the subject looking to one side of the screen, yielding significant horizontal head motion and a classification as d_3.

The symmetrized policy correctly predicts all but one (6/7) action in the test game. The misclassified sequence is longer than usual (over 300 frames) and includes some horizontal head motion in the beginning that appears as shaking in the model. This misclassification may expose a weakness of the temporal segmentation method we use, which is based entirely on the observable actions and game states. Although this sequence is long, it is only the (fairly vigorous) head nod at the very end that is the important display. This situation could be dealt with by incorporating an explicit model of human attention, for example [41].

We performed a second experiment in which the role of *bidder* was exchanged between the same two players and found similar results. The symmetrized policy in this case predicted all 13 actions in the training game, but only 3/5 in the test game. The mispredictions in this case were not due to misclassifications of the behaviors in the sense that the classifications were consistent with others in the training set. They arose instead due to the lack of training data for the POMDP and would be expected to disappear once more data was incorporated.

5.4 Discussion

The experiments we have presented have demonstrated three things. First, the imitation game showed how we can learn models of complex facial expressions with little prior knowledge and no labeled data. This was done by observing causes of the facial expressions in training data only and then predicting the likely causes with over 80 percent accuracy in the test data. The second experiment then showed how, when behaviors are distinct and the task is simple, we can learn the number of behaviors that occur in the data and that are useful to the task being modeled. In 12 experiments, the correct number of gestures was correctly learned in every case. Third, the card matching game demonstrated that we can apply the same learning and solution techniques to a task of realistic size and learn what behaviors (and how many) are being exhibited and what their relationship is to the task. Using synthetic data from simulations, we demonstrated that we can learn a complex transition function and a complex observation function simultaneously and that the resulting model performs close to optimally in simulation and has a structure (number of displays) close to that of the correct model. We then demonstrated how the learning technique on real data from humans playing the card matching game showed how the learned model can predict the actions of humans, and can learn the correct number of displays being used.

In all three of the experiments we have presented, there was never a need to specify what behaviors were to be recognized. The system learned the behaviors that were used within each task and how these behaviors were related to the utility. Thus, by specifying only some of the fully observable aspects of the domain being modeled (such as the rules of the card game), the system can learn the interactions automatically and a new set of behavior models does not need to be reengineered for each new task. For example, suppose the rules of the card game were changed such that the players had to communicate with their hands alone. While a traditional computer vision approach would have to start afresh by building a recognition system for all possible gestures thought (by some experts) to be those that could be used by the participants, our approach could be applied directly and would learn what gestures were being used and why they were being used. This is the primary benefit of this type of learning: No prior knowledge about human behaviors needs to be included, but, rather, can be learned directly from data.

While the results we have presented show the validity of our method from a technical standpoint, a thorough evaluation of the domains that are impacted by this work remains. A significant limitation is that only simulations were used to select actions and gather rewards online. In theory, correct action selection is the only accurate method for validating that the model was learned and solved correctly. Simply predicting actions taken by a human is not sufficient since the learned model could implement a different, yet still optimal, policy

than that used by the human. A second limitation of our current experiments is the use of a fully observed state space (apart from the displays). Additional unobserved variables increase learning complexity and makes temporal segmentation more difficult. A third limitation of our current experiments is that we only use a small number of displays and only allow for merging states during learning. We would like the system to learn a larger number of displays by starting from a small number and splitting states based on, e.g., their predictive power.

6 Conclusion

This paper has shown how partially observable Markov decision processes, or POMDPs, can be used to allow an agent to incorporate actions and utilities into the sensing and representation of visual observations. We have shown how this model provides top-down value-based evidence for the learned probabilistic models and allows us to learn models most conducive for achieving value in a task. One of the key features of this technique is that it does not require labeled data sets. That is, the model makes no prior assumptions about the form or number of nonverbal behaviors used in an interaction, but, rather, *discovers* this from the data during training.

There are three major open questions that remain to be addressed for POMDP modeling of human interactions. First, most interaction tasks will involve state spaces that are significantly larger than we have experimented with in this paper and may be partially or fully unobservable. For example, an assistive system for handwashing used an MDP with over 20 million states [8] and the scalability of the learning method remains to be validated for such larger models. This involves ensuring that we can learn the model parameters for a larger state space and that we can compute good approximate POMDP policies efficiently [29], [50]. However, it is precisely the combination of value-directed learning methods with POMDP solution techniques that will enable the solution of very large POMDPs [43]. The second open question concerns the interplay between a solution for the POMDP and the value-directed structure learning as described in Section 3.3. The strong approximation we used was appropriate for the examples we have examined, but should be relaxed (using, e.g., [29]). More complex structure learning techniques would be required for this learning. The third open question involves the representational power of the observation function. This should be sufficient to distinguish what is necessary to recognize within a particular task. That is, the features used for modeling video sequences of human displays must be able to distinguish what is needed for performance in the task. It remains to be verified if our CHMM-based observation function is sufficient for a wide range of tasks.

Another interesting avenue for future research is the use of the POMDP models in active vision systems [17]. The trade-off between behavior recognition and resource use can be explicitly addressed by a POMDP model and, coupled with the behavior learning techniques we have presented in this paper, would form a possible solution to the active vision problem.

We are currently applying POMDP models to assisted living tasks in which a POMDP-based system helps a cognitively disabled person complete activities of daily living [30]. POMDP models are well suited to this environment since they model the stochastic nature of user behavior, the need to trade off various objective criteria (e.g., task completion, caregiver burden, user frustration, and independence) and the need to tailor guidance to specific individuals and circumstances [8].

Acknowledgments

The authors would like to thank Don Murray, Pantelis Elinas, Pascal Poupart, David Lowe, and David Poole for invaluable help and suggestions. This work was supported by grants from the Natural Sciences and Engineering and Research Council of Canada and from the Institute for Robotics and Intelligent Systems, a Canadian Network of Centres of Excellence.

References

[1] K.J. Åström, "Optimal Control of Markov Decision Processes with Incomplete State Estimation," *J. Math. Analysis and Applications,* vol. 10, pp. 174-205, 1965.

[2] M.S. Bartlett, G. Littlewort, B. Braathen, T.J. Sejnowski, and J.R. Movellan, "A Prototype for Automatic Recognition of Spontaneous Facial Actions," *Advances in Neural Information Processing Systems,* vol. 15, pp. 382-386, 2003.

[3] P.N. Belhumeur, J.P. Hespanha, and D.J. Kriegman, "Eigenfaces versus Fisherfaces: Recognition Using Class Specific Linear Projections," *IEEE Trans. Pattern Analysis and Machine Intelligence,* vol. 19, no. 7, pp. 711-720, July 1997.

[4] R.E. Bellman, *Dynamic Programming*. Princeton Univ. Press, 1957.

[5] Y. Bengio and P. Frasconi, "Input-Output HMMs for Sequence Processing," *IEEE Trans. Neural Networks,* vol. 7, no. 5, pp. 1231-1249, Sept. 1996.

[6] M. Black and Y. Yacoob, "Tracking and Recognizing Rigid and Nonrigid Facial Motions Using Local Parametric Models of Image Motions," *Int'l J. Computer Vision,* vol. 25, no. 1, pp. 23-48, 1997.

[7] A.F. Bobick and J.W. Davis, "The Recognition of Human Movement Using Temporal Templates," *IEEE Trans. Pattern Analysis and Machine Intelligence,* vol. 23, no. 3, pp. 257-267, Mar. 2001.

[8] J. Boger, J. Hoey, P. Poupart, C. Boutilier, G. Fernie, and A. Mihailidis, "A Planning System Based on Markov Decision Processes to Guide People with Dementia through Activities of Daily Living," *IEEE Trans. Information Technology in Biomedicine,* vol. 10, no. 2, pp. 323-333, Apr. 2006.

[9] C. Boutilier, T. Dean, and S. Hanks, "Decision Theoretic Planning: Structural Assumptions and Computational Leverage," *J. Artificial Intelligence Research,* vol. 11, pp. 1-94, 1999.

[10] M. Brand, "Learning Concise Models of Human Activity from Ambient Video via a Structure-Inducing M-Step Estimator," Technical Report TR-97-25, Mitsubishi Electric Research Laboratory, Nov. 1997.

[11] M. Brand, N. Oliver, and A. Pentland, "Coupled Hidden Markov Models for Complex Action Recognition," *Proc. Int'l Conf. Computer Vision and Pattern Recognition,* pp. 994-999, 1997.

[12] C. Bregler, "Learning and Recognising Human Dynamics in Video Sequences," *Proc. IEEE Conf. Computer Vision and Pattern Recognition,* pp. 568-574, 1997.

[13] P. Carbonetto, N. de Freitas, P. Gustafson, and N. Thompson, "Bayesian Feature Weighting for Unsupervised Learning with Application to Object Recognition," *Proc. Ninth Int'l Workshop Artificial Intelligence and Statistics,* pp. 122-128, Jan. 2003.

[14] *Embodied Conversational Agents,* J. Cassell et al., eds. MIT Press, 2000.

[15] L. Chrisman, "Reinforcement Learning with Perceptual Aliasing: The Perceptual Distinctions Approach," *Proc. 10th Nat'l Conf. Artificial Intelligence,* pp. 183-188, 1992.

[16] B. Clarkson and A. Pentland, "Unsupervised Clustering of Ambulatory Audio and Video," *Proc. Int'l Conf. Acoustics, Speech, and Signal Processing,* 1999.

[17] T. Darrell and A.P. Pentland, "Active Gesture Recognition Using Partially Observable Markov Decision Processes," *Proc. 13th IEEE Int'l Conf. Pattern Recognition,* 1996.

[18] T.J. Darrell, I.A. Essa, and A.P. Pentland, "Task-Specific Gesture Analysis in Real-Time Using Interpolated Views," *IEEE Trans. Pattern Analysis and Machine Intelligence,* vol. 18, no. 12, pp. 1236-1242, Dec. 1996.

[19] A.P. Dempster, N.M. Laird, and D.B. Rubin, "Maximum Likelihood from Incomplete Data Using the EM Algorithm," *J. Royal Statistical Soc. B,* vol. 39, pp. 1-38, 1977.
[20] G. Donato, M.S. Bartlett, J.C. Hager, P. Ekman, and T.J. Sejnowski, "Classifying Facial Actions," *IEEE Trans. Pattern Analysis and Machine Intelligence,* vol. 21, no. 10, pp. 974-989, Oct. 1999.
[21] I.A. Essa and A.P. Pentland, "Coding Analysis, Interpretation, and Recognition of Facial Expressions," *IEEE Trans. Pattern Analysis and Machine Intelligence,* vol. 19, no. 7, pp. 757-763, July 1997.
[22] S. Fine, Y. Singer, and N. Tishby, "The Hierarchical Hidden Markov Model: Analysis and Applications," *Machine Learning,* vol. 32, no. 1, pp. 41-62, 1998.
[23] D.J. Fleet, M.J. Black, Y. Yacoob, and A.D. Jepson, "Design and Use of Linear Models for Image Motion Analysis," *Int'l J. Computer Vision,* vol. 36, no. 3, pp. 171-193, 2000.
[24] A.J. Fridlund, *Human Facial Expression: An Evolutionary View.* Academic Press, 1994.
[25] B. Galantucci, "An Experimental Study of the Emergence of Human Communication Systems," *Cognitive Science,* vol. 29, pp. 737-767, 2005.
[26] J. Hoey, "Decision Theoretic Learning of Human Facial Displays and Gestures," PhD thesis, Univ. of British Columbia, 2004.
[27] J. Hoey and J.J. Little, "Representation and Recognition of Complex Human Motion," *Proc. IEEE Conf. Computer Vision and Pattern Recognition,* pp. 752-759, June 2000.
[28] J. Hoey and J.J. Little, "Bayesian Clustering of Optical Flow Fields," *Proc. Int'l Conf. Computer Vision,* pp. 1086-1093, Oct. 2003.
[29] J. Hoey and P. Poupart, "Solving POMDPs with Continuous or Large Discrete Observation Spaces," *Proc. Int'l Joint Conf. Artificial Intelligence,* pp. 1332-1338, July 2005.
[30] J. Hoey, P. Poupart, C. Boutilier, and A. Mihailidis, "POMDP Models for Assistive Technology," *Proc. AAAI Fall Symp. Caring Machines: AI in Eldercare,* 2005.
[31] J. Hoey, R. St-Aubin, A. Hu, and C. Boutilier, "SPUDD: Stochastic Planning Using Decision Diagrams," *Proc. Uncertainty in Artificial Intelligence,* pp. 279-288, 1999.
[32] E. Hunter, J. Schlenzig, and R. Jain, "Posture Estimation in Reduced-Model Gesture Input Systems," *Proc. Int'l Workshop Automatic Face- and Gesture-Recognition,* pp. 290-295, 1995.
[33] T. Jebara and A.P. Pentland, "Action Reaction Learning: Automatic Visual Analysis and Synthesis of Interactive Behaviour," *Proc. Int'l Conf. Vision Systems,* pp. 273-292, 1999.
[34] R.M. Krauss and S. Glucksberg, "Social and Nonsocial Speech," *Scientific Am.,* vol. 236, pp. 100-105, 1977.
[35] A. Lanitis, C.J. Taylor, and T.F. Cootes, "Automatic Interpretation and Coding of Face Images Using Flexible Models," *IEEE Trans. Pattern Analysis and Machine Intelligence,* vol. 19, no. 7, pp. 743-756, July 1997.
[36] C. Li and G. Biswas, "Temporal Pattern Generation Using Hidden Markov Model Based Unsupervised Classification," *Advances in Intelligent Data Analysis,* 1999.
[37] S.X. Liao and M. Pawlak, "On the Accuracy of Zernike Moments for Image Analysis," *IEEE Trans. Pattern Analysis and Machine Intelligence,* vol. 20, no. 12, pp. 1358-1364, Dec. 1998.
[38] D. McNeill, *Hand and Mind: What Gestures Reveal about Thought.* Univ. of Chicago Press, 1992.
[39] K.P. Murphy, "Dynamic Bayesian Networks: Representation, Inference and Learning," PhD thesis, Computer Science Division, Univ. of California Berkeley, July 2002.
[40] N. Oliver, A. Garg, and E. Horvitz, "Layered Representations for Learning and Inferring Office Activity from Multiple Sensory Channels," *Int'l J. Computer Vision and Image Understanding,* vol. 96, pp. 163-180, 2004.
[41] T. Paek and E. Horvitz, "Conversation as Action under Uncertainty," *Proc. Conf. Uncertainty in Artificial Intelligence,* June 2000.
[42] A. Pentland, "Looking at People: Sensing for Ubiquitous and Wearable Computing," *IEEE Trans. Pattern Analysis and Machine Intelligence,* vol. 22, no. 1, pp. 107-119, Jan. 2000.
[43] P. Poupart and C. Boutilier, "Value-Directed Compression of POMDPs," *Advances in Neural Information Processing Systems,* vol. 15, pp. 1547-1554, 2003.
[44] A. Prata and W.V.T. Rusch, "Algorithm for Computation of Zernike Polynomials Expansion Coefficients," *Applied Optics,* vol. 28, no. 4, pp. 749-754, Feb. 1989.
[45] L.R. Rabiner and B.H. Huang, *Fundamentals of Speech Recognition.* Prentice Hall, 1993.
[46] J.A. Russell and J.M. Fernández-Dols, "What Does Facial Expression Mean?" *The Psychology of Facial Expression,* pp. 3-30, 1997.
[47] J. Schlenzig, E. Hunter, and R. Jain, "Vision Based Hand Gesture Interpretation Using Recursive Estimation," *Proc. Asilomar Conf. Signals, Systems, and Computation,* pp. 394-399, Oct. 1994.
[48] E.P. Simoncelli, E.H. Adelson, and D.J. Heeger, "Probability Distributions of Optical Flow," *Proc. Int'l Conf. Computer Vision and Pattern Recognition,* pp. 310-315, 1991.
[49] P. Smyth, "Clustering Sequences with Hidden Markov Models," *Advances in Neural Information Processing Systems,* vol. 10, 1997.
[50] M.T.J. Spaan and N. Vlassis, "Perseus: Randomized Point-Based Value Iteration for POMDPs," *J. Artificial Intelligence Research,* vol. 24, pp. 195-220, 2005.
[51] T. Starner and A.P. Pentland, "Visual Recognition of American Sign Language Using Hidden Markov Models," *Proc. Int'l Workshop Automatic Face and Gesture Recognition,* pp. 189-194, 1995.
[52] R. Sutton and A.G. Barto, *Reinforcement Learning: An Introduction.* MIT Press, 1998.
[53] C.-H. Teh and R.T. Chin, "On Image Analysis by the Methods of Moments," *IEEE Trans. Pattern Analysis and Machine Intelligence,* vol. 10, no. 4, pp. 496-513, July 1988.
[54] S. Thrun, "Probabilistic Algorithms in Robotics," *AI Magazine,* vol. 21, no. 4, pp. 93-109, 2000.
[55] Y. Tian, T. Kanade, and J.F. Cohn, "Recognizing Action Units for Facial Expression Analysis," *IEEE Trans. Pattern Analysis and Machine Intelligence,* vol. 23, no. 2, Feb. 2001.
[56] M. Turk and A.P. Pentland, "Eigenfaces for Recognition," *J. Cognitive Neuroscience,* vol. 3, no. 1, pp. 71-86, 1991.
[57] J. Williams, P. Poupart, and S. Young, "Factored Partially Observable Markov Decision Processes for Dialogue Management," *Proc. IJCAI Workshop Knowledge and Reasoning in Practical Dialogue Systems,* pp. 76-82, Aug. 2005.

Jesse Hoey received the BSc degree in physics from McGill University in Montreal, Canada, and the MSc degree in physics and the PhD degree in computer science from the University of British Columbia, Vancouver, Canada. He is a lecturer in the School of Computing at the University of Dundee, Scotland, and an adjunct scientist at the Toronto Rehabilitation Institute in Toronto, Canada. His research focuses on planning and acting in large-scale, real-world uncertain domains using video observations. In particular, he works on applying decision theoretic planning, computer vision, and machine learning techniques to adaptive assistive technologies in health care.

James J. Little received the AB degree from Harvard College in 1972 and the MSc and PhD degrees in computer science from the University of British Columbia in 1980 and 1985. From 1985 to 1988, he was a research scientist at the MIT Artificial Intelligence Laboratory. Currently, he is a professor of computer science at the University of British Columbia. His research interests include computational vision, robotics, and spatio-temporal information systems. Particular interests are stereo, motion, tracking, mapping, and motion interpretation. He is a member of the IEEE and the IEEE Computer Society.